Nigerian Journal of Theoretical and Environmental Physics (NJTEP)
ISSN Print: 3026-9601
ISSN Online: 1597-9849
DOI: https://doi.org/10.62292/njtep.v3i3.2025.96
Volume 3(3), September 2025

Spatial and Probabilistic Assessment of Radiation and Cancer Risk in Nigerian Seaports

Egagifo, O., *Orute, D., Oyovwevotu, O., Teghware, A. and Agbalagba, E.

Department of Physics, Federal University of Petroleum Resources, Effurun, Delta Sate, Nigeria.

*Corresponding author's email: orute.destiny@fupre.edu.ng

ABSTRACT
Background ionizing radiation (BIR) in seaport environments contributes to public radiological exposure, yet few studies have quantified this risk in Nigerian ports. This study assessed BIR, annual effective dose equivalent (AEDE), and excess lifetime cancer risk (ELCR) across Warri, Koko, and Burutu seaports. Field measurements were collected at 15, 10, and 7 locations per port, respectively. Descriptive analysis revealed mean BIR values of 0.010 ± 0.002 μSvh⁻¹ (Warri), 0.009 ± 0.001 μSvh⁻¹ (Koko), and 0.012 ± 0.002 μSvh⁻¹ (Burutu), with corresponding AEDE estimates well below the 1 mSvy⁻¹ public exposure limit. Mean ELCR values ranged from 0.206×10^{-3} (Koko) to 0.251×10^{-3} (Burutu), approaching the UNSCEAR reference level of 0.29×10^{-3}. Burutu exhibited the highest ELCR, likely due to localized sediment retention zones and port-specific operational features, despite its small size and limited infrastructure. Monte Carlo simulations incorporating instrument uncertainty confirmed the robustness of ELCR estimates, while spatial mapping highlighted micro-zonal hotspots consistent with measured values. Comparison with Onne Port indicated substantially lower ELCRs at the studied seaports, emphasizing the importance of site-specific risk assessments. These findings demonstrate that, although current exposures are within regulatory limits, continued monitoring is recommended, particularly in areas with elevated BIR. The study is limited by its single-season field measurements and small sample size, which may constrain broader generalization. Nonetheless, the combined spatial and probabilistic approach provides a robust baseline radiological data critical for environmental management and public health policy in Nigerian coastal ports.

Keywords:
Background ionizing radiation,
Seaports,
Excess lifetime cancer risk,
Monte Carlo simulation,
Spatial mapping,
Public dose assessment.

INTRODUCTION

Natural background ionizing radiation (BIR) originates from terrestrial radionuclides particularly ^{40}K, ^{238}U and ^{232}Th as well as cosmic rays, with additional contributions in some settings from anthropogenic activities (Ononugbo & Anekwe 2020). Quantifying BIR and translating ambient dose rates into public-health metrics such as annual effective dose (AED) and excess lifetime cancer risk (ELCR) is central to environmental radiological protection, following international guidance (UNSCEAR, 2020). Modern radiological assessments increasingly adopt probabilistic approaches, including Monte Carlo simulation, to propagate measurement variability, instrument uncertainty, and exposure assumptions (Kalospyros et al., 2021; Kalankesh et al., 2024; Biere et al., 2025).

This study was conducted across three seaports in Delta State, Nigeria-Warri, Koko, and Burutu located within the western Niger Delta region. The area spans approximately longitude 5°41′E to 5°48′E and latitude 5°30′N to 5°36′N, characterized by low-lying terrain, tidal river systems, and a tropical monsoon climate with heavy rainfall between March and October (Avwiri et al., 2015; Okoduwa & Amaechi, 2024). Geological variability, sediment transport, and coastal dynamics determine the baseline distribution of natural radionuclides (Kotb et al., 2023), while port activities such as; cargo handling, scrap storage, fuel logistics, and radiological screening can locally modify exposure patterns (Avwiri, Mgbemere, & Ononugbo, 2024). Warri port, the largest, handles high cargo throughput and petroleum-related logistics; Koko port primarily handles agricultural and bulk cargo with relatively lower industrial activity; Burutu port is smaller and serves as a minor shipping hub with limited infrastructure. These differences guided a stratified sampling design allocating 15, 10, and 7 measurement points, respectively, reflecting both port size and environmental heterogeneity. The slightly lower number of points in Koko and Burutu was also influenced by limited accessibility in certain operational areas of the ports, which restricted safe placement of measurement instruments while maintaining representativeness across functional micro-zones. Regional studies in Nigeria demonstrate measurable natural radioactivity in soils, water, and sediments, but most prior work has relied on deterministic point estimates rather than spatially explicit, uncertainty-aware analysis (Agbalagba, Avwiri, & Ononugbo, 2013; Omeje et al., 2020; Mbonu & Ben, 2021; Eke & Amakom, 2022; Isinkaye & Ajiboye, 2022; Esi et al., 2024; Odelami et al., 2024; Adedokun et al., 2025). Spatially explicit analyses, including kernel density estimation (KDE), provide a powerful approach to visualize gradients in radiation intensity, while probabilistic simulations, such as Monte Carlo methods, allow robust estimation of ELCR with uncertainty propagation (Azhdarpoor et al., 2021; Badeenezhad et al., 2023; Mtshawu et al., 2023; Hao et al., 2024).

Despite these methodological advances, comprehensive, reproducible assessments that combine dense, port-micro-zone sampling, KDE-based spatial analysis, and Monte Carlo propagation of measurement and parameter uncertainty remain absent for Nigerian seaports. This study addresses that gap by conducting a spatially stratified survey of background dose rates across Warri, Koko, and Burutu ports. In-situ measurements of BIR levels were done, KDE with contour overlay was applied to visualize spatial gradients in radiation intensity, and Monte Carlo simulation was used to estimate ELCR, following accepted calculation chains and uncertainty propagation practices. The combined spatial-probabilistic approach aligns with established precedent for robust evidence generation (Chatzipapas et al. 2020; Kalospyros et al., 2021; Mtshawu et al., 2023; Kalankesh et al., 2024) and is intended to produce transparent, reproducible results that can guide monitoring priorities, occupational protection, and community health decisions in Nigerian port contexts (Agbalagba et al., 2013; Avwiri, Mgbemere, & Ononugbo, 2024).

MATERIALS AND METHODS

Materials

A total of 32 sampling points were selected across three seaports in Delta State, Nigeria-Warri (15 points), Koko (10 points), and Burutu (7 points) using a stratified spatial design to capture radiological variability across functional zones within each port. Each port was subdivided into three operational zones: Entrance areas (e.g., access roads, gates), Jetty/Berthing zones (e.g., docking platforms, quay sides), and Storage/Cargo handling zones (e.g., container yards, warehouses). Sampling intervals ranged from 50 to 150 meters depending on site accessibility and structural layout. Coordinates for each sampling point were recorded using a GARMIN 76 GPS device and projected in the WGS 1984 / UTM Zone 31N system. This stratification ensured spatial coverage across high-traffic, legacy infrastructure, and sediment-prone areas, enabling robust comparison of radiological exposure across port functions. Radiation measurements were conducted using a Digilert 100 nuclear radiation monitor (S.E. International Inc., USA), equipped with a Geiger-Müller tube for gamma ray detection (Orduvwe et al., 2025). Measurements were taken three times at each sampling point, and the last reading was recorded as the final value for analysis. Readings were taken 1 meter above ground level between 09:00 a.m and 15:00 p.m local time, following the International Atomic Energy Agency (IAEA) guidelines for environmental gamma surveys (IAEA, 2005, 2019). The Digilert 100 radiation monitor was preset for outdoor gamma-ray detection in μSvh-1 mode, following manufacturer guidelines for ambient environmental surveys. This ensured consistent measurement conditions across all sampling points, although no formal calibration with reference sources was conducted. Also, no averaging of the three readings was logged; values were used directly as recorded. Environmental parameters were noted at each sampling session, including ambient temperature (28–33°C), relative humidity (55–70%), wind speed (<5 km/h), and surface type. Ground surfaces varied across functional zones: Entrance areas (paved roads, compacted gravel), Jetty/Berthing zones (reinforced concrete platforms exposed to tidal water), and Storage/Cargo handling zones (mixed terrain: bare soil, asphalt, container stacks). Documenting these conditions supported interpretation of dose rate variability.

Methods

Sampling Justification and Permissions

The allocation of sampling points-Warri (15), Koko (10), Burutu (7) was based on port size, operational complexity, and accessibility constraints. Warri is the largest and busiest port, Koko is medium-sized, and Burutu is smaller with limited infrastructure. Restricted operational zones limited access at some ports. formal permission from the Nigerian Ports Authority (NPA) was obtained for all authorized areas. The study involved no human or animal subjects, and all procedures complied with institutional and national safety regulations. Hence, this approach ensured representative coverage of functional micro-zones while maintaining safety and compliance.

Environmental Considerations

Environmental parameters recorded at each site included ambient temperature (28–33°C), relative humidity (55–70%), wind speed (<5 km/h), and surface type. Ground surfaces varied across functional zones: Entrance areas (paved roads, compacted gravel), Jetty/Berthing zones (reinforced concrete platforms exposed to tidal water), and Storage/Cargo handling zones (mixed terrain: bare soil, asphalt, container stacks). Documenting these conditions helped minimize confounding effects and supported interpretation of observed dose rate variability.

Radiological Risk Assessment

Measured BIR values were used to calculate two radiological risk metrics:

*Annual Effective Dose Equivalent (AEDE)**:***

$$AEDE(mSvy^{-1}) = BIR(\mu Svh^{-1}) \times 8760 \times 0.7 \times 10^{-6} \quad (1)$$

Where 8760 represents the total hours in a year and 0.7×10^{-6} accounts for the occupancy factor and the unit conversion from μSv to mSv. Effective dose conversion followed ICRP Publication 60 and 147 standards (ICRP, 1991; Harrison et al., 2021).

*Excess Lifetime Cancer Risk (ELCR)**:***

$$ELCR\ (\times 10^{-3}) = AEDE \times average\ duration\ of\ life\ (DL) \times risk\ factor\ (RF) \quad (2)$$

Where 70 years represents the average lifespan and 0.05 Sv^{-1} is the ICRP recommended risk factor for public exposure (ICRP, 1991).

Note: Tables 1–3 present the raw background ionizing radiation (BIR) measurements (μSvh^{-1}) recorded at 15, 10, and 7 sampling points in Warri, Koko, and Burutu ports, respectively. These values represent unprocessed field readings obtained with the calibrated Digilert-100 radiation monitor, and were used as the input dataset for all subsequent statistical and Monte Carlo analysis.

Statistical Analysis

All analysis was conducted using Python 3.13 with open-source libraries (NumPy, Pandas, SciPy, Matplotlib, Seaborn, GeoPandas, Folium): Normality: Shapiro–Wilk test applied to ANOVA residuals rather than raw group distributions; homoscedasticity: Levene's test assessed equality of variances across ports; group comparisons: Welch ANOVA accounted for unequal variances and sample sizes; post-hoc pairwise comparisons used Games–Howell tests; effect sizes: η^2, ω^2, and Cohen's g were computed to evaluate practical significance; exceedance proportions: Binomial Clopper–Pearson intervals were used to quantify uncertainty due to small sample sizes and spatial dependence: Moran's I was computed to detect autocorrelation between sampling points, ensuring ANOVA assumptions were interpreted appropriately.

Monte Carlo Simulation

Monte Carlo simulation was implemented to model uncertainty in ELCR estimates:

Iterations: 10,000

Random seed: 20251014

Distribution: Uniform sampling of measured BIR values per port, with ±3% Gaussian noise to account for instrument variability

Formula: ELCR calculated from AEDE as described above

Scaling: ELCR values multiplied by 10^3 and reported in units of $\times 10^{-3}$ to align with UNSCEAR thresholds

Diagnostics: Histograms, KDE overlays, cumulative percentiles, and convergence checks were performed

Sensitivity analysis: Normal, Triangular, and Bootstrap resampling showed <5% variation in mean ELCR and confidence interval widths, demonstrating robustness.

Spatial Visualization

Spatial distribution of BIR intensity across ports was visualized using kernel density estimation (KDE) with contour overlays. Sampling coordinates were georeferenced in WGS 84 and mapped using GeoPandas and Folium, allowing smooth interpolation of radiation gradients across micro-zones without assuming linearity or stationarity.

RESULTS AND DISCUSSION

Descriptive Statistics of Seaport Background Ionizing Radiation

Tables 1–3 summarize the measured background ionizing radiation (BIR), annual effective dose equivalent (AEDE), and excess lifetime cancer risk (ELCR) across the three Delta Seaports-Warri, Koko, and Burutu. The mean BIR values ranged from 0.009 ± 0.001 μSvh^{-1} (Koko) to 0.012 ± 0.002 μSvh^{-1} (Burutu), with Warri exhibiting an intermediate value of 0.010 ± 0.002 μSvh^{-1}. These values lie within the ICRP's global terrestrial background range (0.01–0.02 μSvh^{-1}) but display mild spatial heterogeneity likely influenced by site-specific lithological characteristics and localized port features.

Table 1: Background ionizing radiation (BIR), annual effective dose equivalent (AEDE) and excess lifetime cancer risk (ELCR × 10⁻³) at Warri Seaport

S/N	Sampling Location	Latitude(°N)	Longitude (°E)	BIR (μSvh⁻¹)	AEDE (mSvy⁻¹)	ELCR × 10⁻³
1	Control Tower	05°31′17″ N	05°44′35″ E	0.009	0.055	0.19
2	NPA Gate	05°31′25″ N	05°44′40″ E	0.009	0.055	0.19
3	New Port 1	05°31′45″ N	05°44′55″ E	0.011	0.067	0.23
4	New Port Shed 2	05°31′52″ N	05°45′05″ E	0.010	0.061	0.21
5	New Port Intel 2	05°31′58″ N	05°45′09″ E	0.011	0.067	0.23
6	New Port Intel 3	05°32′03″ N	05°45′14″ E	0.012	0.074	0.26
7	New Port Berger	05°32′07″ N	05°45′20″ E	0.009	0.055	0.19
8	NPA Fire Station	05°32′10″ N	05°45′28″ E	0.009	0.055	0.19
9	NPA Clinic	05°32′18″ N	05°45′33″ E	0.014	0.086	0.30
10	Flour Mill Cargo Zone	05°32′21″ N	05°45′42″ E	0.011	0.067	0.23
11	Admin Office	05°32′25″ N	05°45′50″ E	0.008	0.049	0.17
12	Commercial Area	05°32′29″ N	05°45′57″ E	0.011	0.067	0.23
13	AMS 2	05°32′33″ N	05°46′05″ E	0.009	0.055	0.19
14	Mosque Area	05°32′37″ N	05°46′12″ E	0.010	0.061	0.21
15	Customs Area	05°32′42″ N	05°46′18″ E	0.009	0.055	0.19
Mean ± SD —		—	—	0.010 ± 0.002	0.062 ± 0.010	0.22 ± 0.04

(Coordinates in WGS 84, DMS format); ELCR values are reported in units of ×10⁻³ for consistency with UNSCEAR thresholds.

Table 2: BIR, AEDE and ELCR × 10⁻³ at Koko Seaport

S/N	Sampling Location	Latitude (°N)	Longitude (°E)	BIR (μSvh⁻¹)	AEDE (mSvy⁻¹)	ELCR × 10⁻³
1	Admin Block	05°58′14″ N	05°45′26″ E	0.010	0.061	0.21
2	Police Station	05°58′17″ N	05°45′31″ E	0.010	0.061	0.21
3	Fire Station	05°58′23″ N	05°45′38″ E	0.011	0.067	0.23
4	Storage Point 1	05°58′29″ N	05°45′44″ E	0.008	0.049	0.17
5	Container Yard	05°58′34″ N	05°45′50″ E	0.008	0.049	0.17
6	Anchoring Point	05°58′38″ N	05°45′55″ E	0.011	0.067	0.23
7	Warehouse	05°58′42″ N	05°46′00″ E	0.010	0.061	0.21
8	Control Tower	05°58′47″ N	05°46′06″ E	0.011	0.067	0.23
9	Storage Point 2	05°58′51″ N	05°46′12″ E	0.008	0.049	0.17
10	Port Gate	05°58′55″ N	05°46′17″ E	0.011	0.067	0.23
Mean ± SD —		—	—	0.010 ± 0.001	0.060 ± 0.009	0.21 ± 0.03

(Coordinates in WGS 84, DMS format); ELCR values are reported in units of ×10⁻³ for consistency with UNSCEAR thresholds.

Table 3: BIR, AEDE and ELCR × 10⁻³ at Burutu Seaport

S/N	Sampling Location	Latitude (°N)	Longitude (°E)	BIR (μSvh⁻¹)	AEDE (mSvy⁻¹)	ELCR × 10⁻³
1	Entrance	05°21′05″ N	05°30′41″ E	0.014	0.086	0.30
2	Storage Point 1	05°21′09″ N	05°30′47″ E	0.013	0.080	0.28
3	Storage Point 2	05°21′14″ N	05°30′52″ E	0.013	0.080	0.28
4	Anchoring Point	05°21′18″ N	05°30′58″ E	0.011	0.067	0.23
5	Wooden Bridge	05°21′22″ N	05°31′03″ E	0.010	0.061	0.21
6	River Level	05°21′27″ N	05°31′08″ E	0.010	0.061	0.21
7	Wreck Area	05°21′32″ N	05°31′14″ E	0.013	0.080	0.28
Mean ± SD —		—	—	0.012 ± 0.002	0.073 ± 0.010	0.25 ± 0.04

(Coordinates in WGS 84, DMS format); ELCR values are reported in units of ×10⁻³ for consistency with UNSCEAR thresholds.

The Box plot analysis (Figure 1) revealed distinct distributional patterns across the ports. Warri and Koko exhibited relatively narrow interquartile ranges (IQRs) with median BIR values centered around 0.010 μSvh⁻¹, indicating consistent background levels with limited dispersion. In contrast, Burutu displayed a higher median BIR and a tighter upper quartile, suggesting elevated radiation levels with reduced variability. Minimal outliers were observed, and strip plot overlays confirmed that most measurements clustered near the median in Warri and Koko, while Burutu values skewed slightly higher. These visual trends complement the descriptive statistics and support the identification of Burutu as a site with a distinct radiological profile.

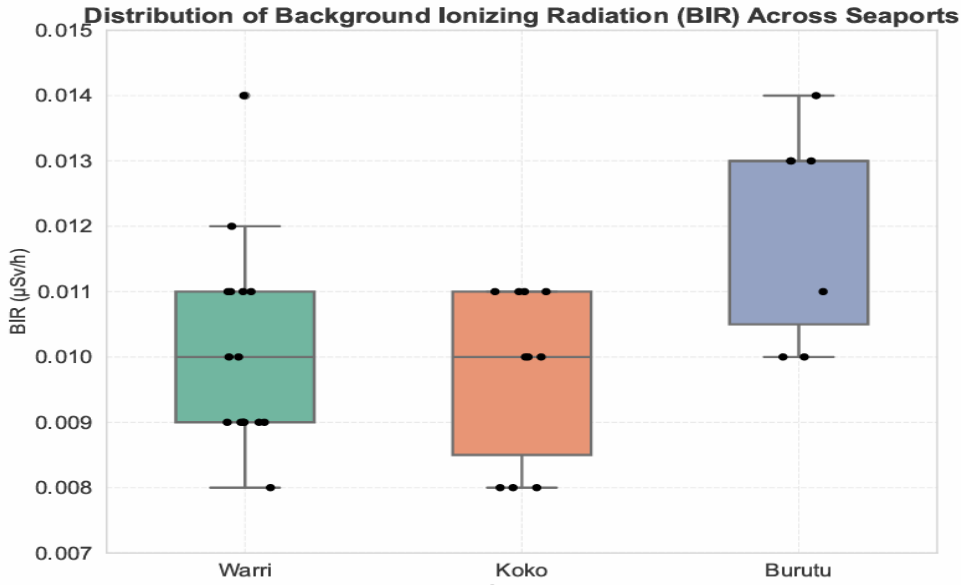

Figure 1: Boxplots of BIR values by Seaports

The corresponding AEDE values indicate annual public exposures of 0.052–0.070 mSvy⁻¹, well below the 1 mSvy⁻¹ public dose limit recommended by the ICRP (Harrison et al., 2021). When translated into lifetime risk, the mean ELCR values ranged from 0.206×10^{-3} (Koko) to 0.251×10^{-3} (Burutu). The observed mean excess lifetime cancer risk (ELCR $\approx 0.20–0.25 \times 10^{-3}$) corresponds to approximately 20–25 potential additional cancer cases per 100,000 exposed individuals over a lifetime, which remains within the global reference limit of 0.29×10^{-3} recommended by UNSCEAR (2020). Benchmarking against Onne Port, Port Harcourt (Avwiri, Mgbemere, & Ononugbo 2024), where ELCR values ranged from 0.17 to 0.509 with a mean of 0.289×10^{-3}, shows that the three Delta seaports exhibited markedly lower ELCRs despite comparable industrial activities. This contrast likely reflects differences in sediment composition, port infrastructure, operational intensity, and environmental management. The slightly elevated ELCR observed at Burutu may be influenced by localized factors such as sediment retention zones and specific docking or anchoring areas, highlighting the need for targeted monitoring and site-specific risk assessment.

Monte Carlo Simulation of Excess Lifetime Cancer Risk

The Monte Carlo simulation (10 000 iterations; seed = 20251014) quantified uncertainty propagation in the ELCR estimates (Table 4). For each port, randomization incorporated the calibration uncertainty of ±3 %, modeled as Gaussian noise around the mean BIR. The resulting kernel density estimates (KDEs), histograms, and cumulative distribution functions (CDFs) exhibited narrow unimodal distributions, indicating stable mean convergence beyond approximately 2 000 iterations.

Table 4: Monte Carlo summary of Excess Lifetime Cancer Risk (ELCR × 10⁻³) for Nigerian seaports (10 000 iterations, seed = 20251014)

Seaport	Mean ELCR ($\times 10^{-3}$)	2.5 % Quantile	Median (50 %)	97.5 % Quantile	Coefficient of Variation (%)	Remarks / Distribution Used
Warri	0.221	0.171	0.221	0.281	9.4	Uniform; convergence by ≈ 3 000 iterations
Koko	0.206	0.171	0.206	0.269	8.7	Uniform; narrow CI shows stable results
Burutu	0.251	0.192	0.251	0.302	10.2	Uniform; slightly higher spread due to smaller n

Note: ELCR values are expressed in $\times 10^{-3}$ units, directly comparable to the analytical threshold (0.29×10^{-3}). Calibration uncertainty was incorporated into the Monte Carlo simulations by applying ±3 % Gaussian noise to each BIR value to represent instrument variability. This adjustment was not applied to the deterministic AEDE and ELCR values in Tables 1–3 to preserve direct comparability with measured field data. Alternative sampling schemes (Normal, Triangular, Bootstrap) varied by less than 5 %, confirming robustness. CI = Confidence Interval.

Among the ports, Burutu demonstrated the widest spread (σ = 0.0009 × 10^{-3}) and highest mean risk (0.251 × 10^{-3}), while Koko showed the narrowest uncertainty band (σ = 0.0005 × 10^{-3}). Figure 2 presents the Monte Carlo diagnostic outputs for Warri Port: running mean convergence, kernel density estimation (KDE), cumulative distribution function (CDF), and histogram of simulated excess lifetime cancer risk (ELCR ×10^{-3}), while comparable plots for Koko and Burutu are provided in the supplementary material alongside the annotated Python pseudocode used for stochastic modeling. The stability of convergence validates the sample adequacy and simulation robustness.

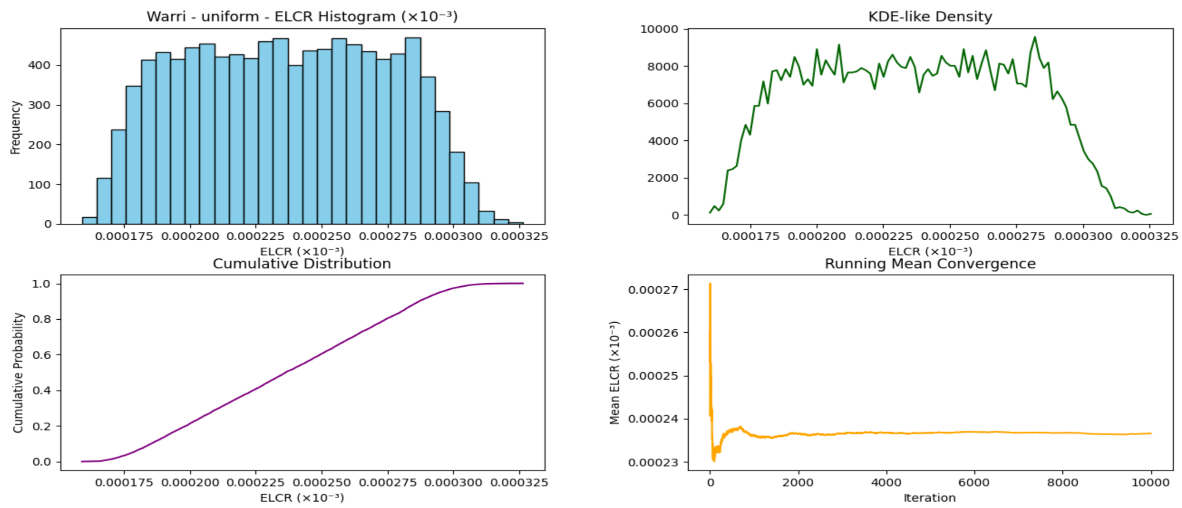

Figure 2: Monte Carlo diagnostics for Warri Port: running mean, KDE, CDF, and ELCR histogram (×10^{-3})

Inter-Port Variability and Statistical Significance

Table 5 summarizes the descriptive and inferential statistics of BIR and ELCR across the three ports. The Welch-adjusted one-way ANOVA revealed a significant difference in mean BIR among ports ($F = 5.003$, $p = 0.0136$), further supported by the non-parametric consistency of the Welch test ($p < 0.01$). This indicates that the variation in BIR across the ports is not due to random fluctuations but reflects genuine spatial disparity.

Table 5: Descriptive statistics and ANOVA summary for background ionizing radiation (BIR) and excess lifetime cancer risk (ELCR) across the three Nigerian seaports

Parameter / Test	Warri	Koko	Burutu	Notes / Statistics
Descriptive Statistics				
Mean ± SD (BIR, µSv h^{-1})	0.010 ± 0.002	0.009 ± 0.001	0.012 ± 0.002	—
Mean ELCR (×10^{-3})	0.221	0.206	0.251	ELCR values in ×10^{-3} units
95 % CI for ELCR (×10^{-3})	0.171 – 0.281	0.171 – 0.269	0.192 – 0.302	—
Coefficient of Variation (%)	9.4	8.7	10.2	—
Welch ANOVA P-value	—	—	3.2 × 10^{-3} (**$p < 0.01$**)	Significant difference among ports
One-Way ANOVA Summary				
Source	—	—	—	SS = 2.254 × 10^{-5}; df = 2; MS = 1.127 × 10^{-5}; F = 5.003; P = 0.0136
Residual	—	—	—	SS = 6.533 × 10^{-5}; df = 29; MS = 2.253 × 10^{-6}

Note: ELCR values are expressed in ×10^{-3} units, directly comparable to the analytical threshold (0.29 × 10^{-3}). Calibration uncertainty (± 3 %) was incorporated into Monte Carlo simulations as Gaussian noise on BIR to represent instrument variability but was not applied to deterministic AEDE and ELCR values in Tables 1–3 to preserve comparability with field data. CI = Confidence Interval.

To assess practical significance, effect size indices (Table 6) were computed: $\eta^2 = 0.257$ and $\omega^2 = 0.200$, both indicative of a moderate practical effect. The Games–Howell post-hoc tests, robust to unequal variances and sample sizes, identified a statistically significant difference between Burutu and Koko ($p = 0.032$), a marginal difference between Burutu and Warri ($p \approx 0.07$), and no difference between Warri and Koko ($p = 0.834$). Collectively, these findings confirm that the higher mean dose at Burutu materially elevates the radiological baseline relative to the other ports.

Table 6: Effect sizes, Welch ANOVA, and Games–Howell post-hoc comparisons for inter-port differences

Test / Comparison	Statistic	Value	Interpretation
Effect Size Estimates			
η^2 (Eta squared)	—	0.257	Moderate effect
ω^2 (Omega squared)	—	0.200	—
Welch ANOVA (Unequal Variance)			
Source = Port	$df_1 = 2$; $df_2 = 15.11$	F = 4.397; P = 0.0313	Partial $\eta^2 = 0.257$
Games–Howell Post-hoc Comparisons			
Burutu vs Koko	Mean diff = 0.0022 ± 0.00074 SE	T = 2.955; df = 11.16; P = 0.032	G = 1.439
Burutu vs Warri	Mean diff = 0.00187 ± 0.00074 SE	T = 2.536; df = 11.27; P = 0.065	G = 1.139
Koko vs Warri	Mean diff = –0.00033 ± 0.00058 SE	T = –0.577; df = 21.53; P = 0.834	G = –0.220

Note: Welch ANOVA and Games–Howell post-hoc tests were used to correct for unequal variances and sample sizes. Effect-size estimates indicate a moderate practical difference in BIR among ports, driven mainly by higher mean values at Burutu Port. P-*values < 0.05 denote statistical significance.*

Residual diagnostics (Figure 3) show a near-normal distribution centered around zero, as confirmed by the Shapiro–Wilk test and QQ plot. However, Levene's test indicated significant heterogeneity of variances ($p < 0.05$), justifying the adoption of Welch ANOVA and Games–Howell post-hoc comparisons.

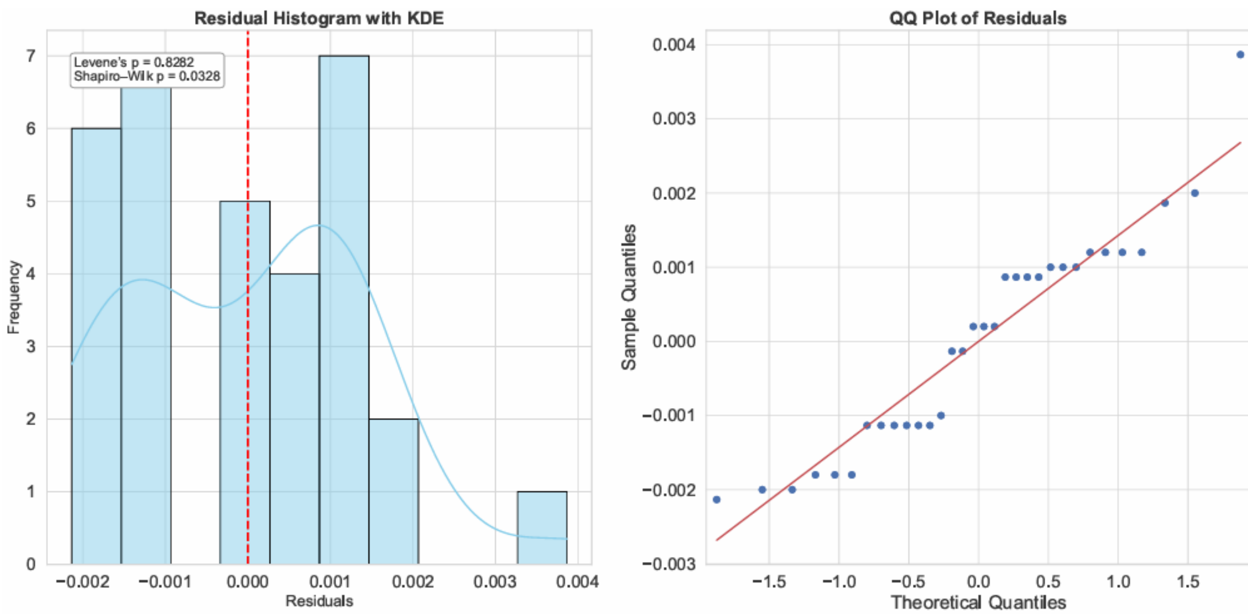

Figure 3: Residual diagnostics showing near-normal distribution; unequal variances confirmed by Levene's test, justifying Welch ANOVA and Games–Howell post-hoc

Spatial Dependence and Exceedance Analysis

Spatial structure was examined using Moran's I statistic (Table 7), which yielded I = 0.1217 ($p = 0.054$). This weak, non-significant spatial autocorrelation suggests approximate independence of BIR values across the sampled sites, an assumption necessary for unbiased inference.

Table 7: Summary of spatial, exceedance, and post-hoc comparative statistics for seaport background ionizing radiation (BIR)

Statistic / Comparison	Estimate ± SE (or %)	95%CI/df	*P*	Interpretation
Moran's I (overall)	0.121659	—	0.054	Weak, non-significant spatial clustering; independence assumption acceptable
Warri – Koko Exceedance (% sites > 0.011 µSv h⁻¹)	13.3 (2/15) vs 0 (0/10)	1.66 – 40.46 / 0 – 30.85	—	Warri slightly higher exceedance; wide CIs → low precision
Burutu Exceedance	57.1 (4/7)	18.41 – 90.10	—	Highest proportion of elevated sites
Games–Howell (Burutu – Koko)	Δ = 0.0022 ± 0.0007 µSv h⁻¹	T = 2.95 / df = 11.16	0.032	Significant difference; Burutu > Koko
Games–Howell (Burutu – Warri)	Δ = 0.0019 ± 0.0007 µSv h⁻¹	T = 2.54 / df = 11.27	0.065	Marginal (p ≈ 0.07); Burutu > Warri
Games–Howell (Koko – Warri)	Δ = –0.0003 ± 0.0006 µSv h⁻¹	T = –0.58 / df = 21.53	0.834	No significant difference

Note: CI = Confidence Interval; SE = Standard Error. Exceedance threshold = 0.011 µSvh⁻¹. Moran's I computed with inverse-distance weighting (999 permutations).

Exceedance analysis based on the regulatory threshold of 0.011 µSvh⁻¹ showed that 57.1 % of Burutu sites exceeded the threshold (95 % CI = 18.4–90.1 %), compared with 13.3 % in Warri and 0 % in Koko. The wide confidence bands reflect limited sampling precision but consistently point to Burutu as the most radiologically elevated port. These findings are visually corroborated by the KDE-based spatial heat map (Figure 4) and the boxplots (Figure 1), which show distinct right-skewed tails for Burutu and tighter central distributions for Koko.

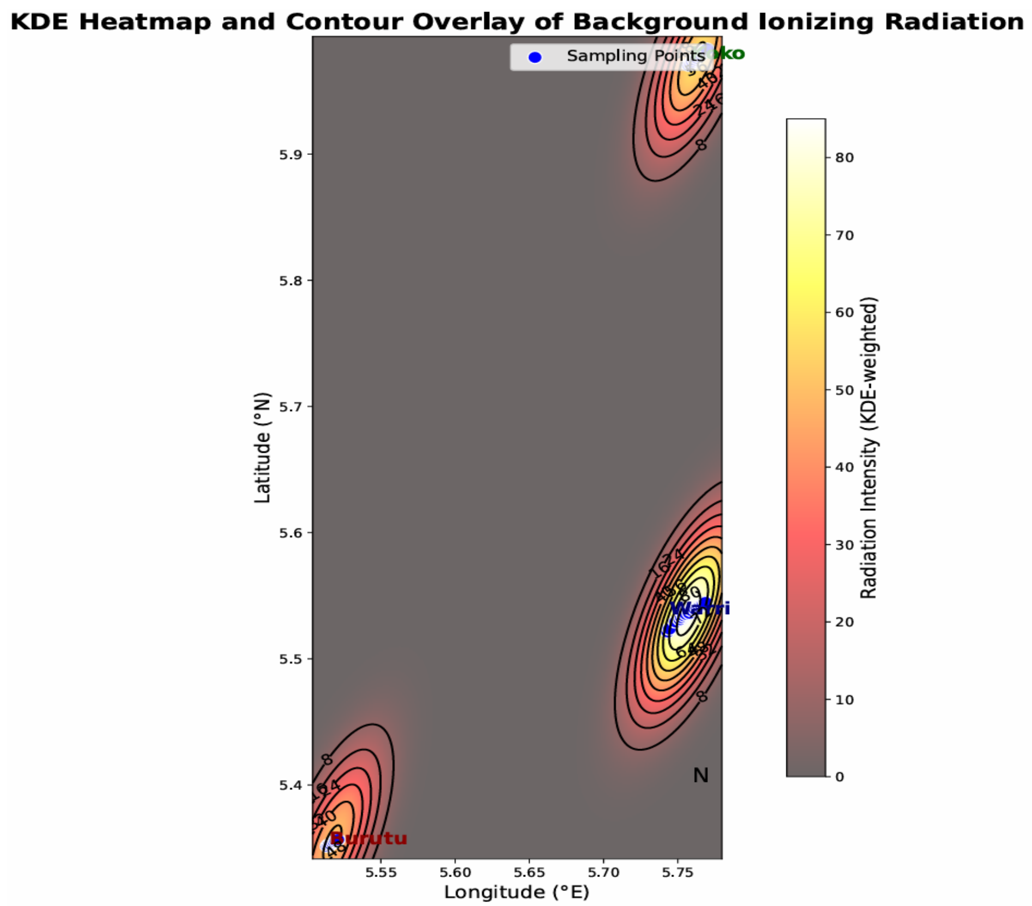

Figure 4: Kernel density estimation (KDE) heat map of spatial BIR distribution

Discussion of Implications

Overall, the statistical and spatial evidence converge on a coherent interpretation: Burutu Port exhibits moderately elevated radiological background levels, plausibly linked to sedimentary radionuclide accumulation, hydrocarbon residues from oil-related activities, and coastal depositional processes. The statistically significant inter-port differences, moderate effect sizes, and high exceedance proportions suggest that these elevations are driven by localized environmental and operational factors rather than a uniform regional background. Although all AEDE values remain below the ICRP's 1 mSv/y public exposure threshold, the proximity of ELCR values to the UNSCEAR reference benchmark (0.29×10^{-3}) raises important considerations for environmental health policy. Specifically, the findings highlight the need for targeted surveillance in micro-zones with persistent industrial inputs, such as anchorage points and sediment retention areas, where cumulative exposure may pose long-term health risks to port workers and nearby communities.

From a public health perspective, even marginal increases in lifetime cancer risk warrant precautionary attention, particularly in vulnerable populations with prolonged occupational or residential exposure. These results support the integration of radiological monitoring into broader environmental health frameworks and occupational safety protocols within port jurisdictions. The demonstrated robustness of Monte Carlo-derived ELCR estimates reinforces the value of probabilistic modeling in regulatory contexts, offering a transparent and reproducible basis for risk communication and evidence-based decision-making (Biere et al., 2025). Furthermore, the spatially resolved baseline established in this study provides a critical reference for future geospatial risk modeling, enabling early detection of radiological anomalies and validation of predictive simulations under evolving industrial and environmental conditions. As Nigeria expands its maritime infrastructure, embedding such spatial-probabilistic assessments into routine environmental audits will be essential for safeguarding public health and ensuring compliance with international radiological protection standards.

CONCLUSION

This study assessed background ionizing radiation (BIR), annual effective dose equivalent (AEDE), and excess lifetime cancer risk (ELCR) across Warri, Koko, and Burutu seaports in Delta State, Nigeria. BIR values ranged 0.008–0.014 μSvh^{-1}, with ELCR estimates of 0.206–0.251 $\times 10^{-3}$, all below international safety thresholds. Burutu Port showed slightly elevated values, likely due to localized sediment retention and docking areas, despite its limited infrastructure. Welch ANOVA and Games–Howell tests confirmed significant inter-port differences, while Monte Carlo simulations incorporating calibration uncertainty provided robust ELCR estimates. KDE mapping and Moran's I highlighted micro-zonal hotspots with weak overall spatial autocorrelation. Benchmarking against Onne Port indicated lower radiological risk at the studied seaports, emphasizing the need for site-specific environmental assessment. Overall, these results support ongoing monitoring of identified hotspots and demonstrate that integrating deterministic measurements, probabilistic modeling, and spatial analysis offers a reproducible framework for coastal port radiological surveillance and risk management. This study was limited by the modest number of sampling points and single-season observations; future work should incorporate multi-season datasets, include more ports, and evaluate radionuclide pathways to strengthen the predictive model.

REFERENCES

Adedokun, M. B., Ibitoye, A. Z., Saghana, V., & Olusola, O. I. (2025). Assessment of radiological risks in using coastal sediments as building materials in Lagos, Nigeria. DISCOVER ENVIRONMENT, 3, Article 80. https://doi.org/10.1007/s44274-025-00265-z

Agbalagba, E. O., Avwiri, G. O., & Ononugbo, C. P. (2013). Activity concentration and radiological impact assessment of ^{226}Ra, ^{228}Ra and ^{40}K in drinking waters from OML 30, 58 and 61 oil fields and host communities in the Niger Delta region of Nigeria. JOURNAL OF ENVIRONMENTAL RADIOACTIVITY, 116, 197–200. https://doi.org/10.1016/j.jenvrad.2012.08.017

Azhdarpoor, A., Hoseini, M., Shahsavani, S., Shamsedini, N., & Gharehchahi, E. (2021). Assessment of excess lifetime cancer risk and risk of lung cancer due to exposure to radon in a Middle Eastern city in Iran. RADIATION MEDICINE AND PROTECTION, 2(1), 18–24. https://doi.org/10.1016/j.radmp.2021.07.002

Avwiri, G. O., & Oghenevovwero, E. E. (2015). Survey of background ionization radiation level in Burutu L.G.A., coastal area of Delta State, Nigeria. JOURNAL OF APPLIED PHYSICAL SCIENCE INTERNATIONAL, 2(2), 72–78. https://ikprress.org/index.php/JAPSI/article/view/2870

Avwiri, G. O., Mgbemere, C. J., & Ononugbo, C. P. (2024). Evaluation of background ionizing radiation and its associated health hazards in Onne Port Complex, Port Harcourt. RESEARCH JOURNAL OF PURE SCIENCE AND TECHNOLOGY, 7(2), 1–9.

Badeenezhad, A., Soleimani, H., Shahsavani, S., Parseh, I., Mohammadpour, A., & Azadbakht, O. (2023). Comprehensive health risk analysis of heavy metal pollution using water quality indices and Monte Carlo simulation in R software. SCIENTIFIC REPORTS, 13, 15817. https://doi.org/10.1038/s41598-023-43161-3

Biere, P. E., Emumejaye, K., Aluko, T. O., Nwaobia, A. G., Okeyode, I. C., & Mustapha, O. A. (2025). An evaluation of excess lifetime cancer risk from indoor and outdoor radiation exposure in Okutukutu Computer Village, Yenagoa, Bayelsa State, Nigeria: A Monte Carlo simulation approach. NIGERIAN JOURNAL OF THEORETICAL AND ENVIRONMENTAL PHYSICS, 3(1), 10–16. https://doi.org/10.62292/njtep.v3i1.2025.66

Chatzipapas, K. P., Papadimitroulas, P., Emfietzoglou, D., Kalospyros, S. A., Hada, M., Georgakilas, A. G., & Kagadis, G. C. (2020). Ionizing radiation and complex DNA damage: Quantifying the radiobiological damage using Monte Carlo simulations (Review). CANCERS, 12(4), 799. https://doi.org/10.3390/cancers12040799

Eke, B. C., & Amakom, C. M. (2022). Radiological dose assessment due to the presence of NORMs in the top soil of the Imo State Polytechnic, Imo State, Nigeria. ENVIRONMENTAL HEALTH INSIGHTS, 16, 1–12. https://doi.org/10.1177/11786302221137219

Esi, O. E., Avwiri, G. O., Sylvanus, O. A., & Onwudiwe, D. C. (2024). Radiometric survey of sediments and health risk assessments from the southern coastal area of Delta State, Nigeria. HELIYON, 10(5), e26805. https://doi.org/10.1016/j.heliyon.2024.e26805

Hao, Y., et al. (2024). A Monte Carlo simulation dataset of radiation field parameters for a simple nuclear facility scenario. SCIENTIFIC DATA. https://doi.org/10.1038/s41597-024-03799-8

Harrison, J. D., Balonov, M., Bochud, F., Martin, C., Menzel, H.-G., Ortiz-Lopez, P., Smith-Bindman, R., Simmonds, J. R., & Wakeford, R. (2021). Use of dose quantities in radiological protection (ICRP Publication 147). ANNALS OF THE ICRP, 50(1), 9–82. https://doi.org/10.1177/0146645320911864

International Commission on Radiological Protection (ICRP). (1991). 1990 RECOMMENDATIONS OF THE INTERNATIONAL COMMISSION ON RADIOLOGICAL PROTECTION (ICRP PUBLICATION 60). ANNALS OF THE ICRP, 21(1–3). https://doi.org/10.1016/0146-6453(91)90001-3

International Atomic Energy Agency. (2005). ENVIRONMENTAL AND SOURCE MONITORING FOR PURPOSES OF RADIATION PROTECTION (IAEA Safety Standards Series No. RS-G-1.8). Vienna: International Atomic Energy Agency. https://www.iaea.org/publications/7176/environmental-and-source-monitoring-for-purposes-of-radiation-protection

International Atomic Energy Agency. (2019). GUIDELINES ON SOIL AND VEGETATION SAMPLING FOR RADIOLOGICAL MONITORING (Technical Reports Series No. 486). Vienna: International Atomic Energy Agency. https://www.iaea.org/publications/12219/guidelines-on-soil-and-vegetation-sampling-for-radiological-monitoring

Isinkaye, M. O., & Ajiboye, O. A. (2022). Natural radioactivity in surface soil of urban settlements in Ekiti State, Nigeria: Implications for radiological health risks. ARABIAN JOURNAL OF GEOSCIENCES, 15, 557. https://doi.org/10.1007/s12517-022-09835-4

Kalankesh, L. R., Mosaferi, M., Khajavian, N., Sarvari, B., & Zarei, A. (2024). Simulation of excess lifetime lung cancer risk due to indoor radon exposure in Eastern Iran—Monte Carlo simulation method. JOURNAL OF RADIATION RESEARCH AND APPLIED SCIENCES, 17(4), 101193. https://doi.org/10.1016/j.jrras.2024.101193

Kalospyros, S. A., Gika, V., Nikitaki, Z., Kalamara, A., Kyriakou, I., Emfietzoglou, D., Kokkoris, M., & Georgakilas, A. G. (2021). Monte Carlo simulation-based calculations of complex DNA damage for incidents of environmental ionizing radiation exposure. APPLIED SCIENCES, 11(19), 8985. https://doi.org/10.3390/app11198985

Kotb, N. A., Abd El Ghany, M. S., & El-Sayed, A. A. (2023). Radiological assessment of different monazite grades after mechanical separation from black sand. SCIENTIFIC REPORTS, 13, 15389. https://doi.org/10.1038/s41598-023-42287-8

Mbonu, C. C., & Ben, U. C. (2021). Assessment of radiation hazard indices due to natural radioactivity in soil samples from Orlu, Imo State, Nigeria. HELIYON, 7(8), e07812. https://doi.org/10.1016/j.heliyon.2021.e07812

Mtshawu, B., Bezuidenhout, J., & Kilel, K. K. (2023). Spatial autocorrelation and hotspot analysis of natural radionuclides to study sediment transport. JOURNAL

OF ENVIRONMENTAL RADIOACTIVITY, 264, 107207. https://doi.org/10.1016/j.jenvrad.2023.107207

Odelami, K. A., Oladipo, M. O. A., Onoja, M. A., Musa, Y., & Aremu, S. O. (2024). Assessment of radiological contamination due to gold mining in soil and food crops of Babban Tsauni, Gwagwalada, Nigeria. RADIATION PROTECTION DOSIMETRY, 200(20), 1961–1970. https://doi.org/10.1093/rpd/ncae207

Okoduwa, A. K., & Amaechi, C. F. (2024). Spatial distribution of climate change variables (rainfall and temperature): Case study of Delta State, Nigeria [Preprint]. RESEARCH SQUARE. https://doi.org/10.21203/rs.3.rs-4202634/v1

Omeje, M., Adewoyin, O. O., Joel, E. S., Ijeh, B. I., & Oha, I. A. (2020). Spatial distribution of gamma radiation dose rates from natural radionuclides and its radiological hazards in sediments along River Iju, Ogun State, Nigeria. METHODSX, 7, 101086. https://doi.org/10.1016/j.mex.2020.101086

Ononugbo, C. P., & Anekwe, U. (2020). Background gamma radiation in Nigerian market environment. AMERICAN JOURNAL OF ENVIRONMENTAL SCIENCES, 16(3), 48–54. https://doi.org/10.3844/ajessp.2020.48.54

Orduvwe, T. A., Avwiri, G. O., & Oghenenyerhovwo, A. E. (2025). Radiological risk assessment among occupational health workers in selected radiological centres in Warri City, Nigeria. TRENDS IN SOCIAL SCIENCES, 1(1), 1–9. https://doi.org/10.21124/tss.2025.01.09

United Nations Scientific Committee on the Effects of Atomic Radiation (UNSCEAR). (2020). SOURCES, EFFECTS AND RISKS OF IONIZING RADIATION: UNSCEAR 2020 REPORT TO THE GENERAL ASSEMBLY WITH SCIENTIFIC ANNEXES (VOLS. I–II). United Nations. https://www.unscear.org/unscear/en/publications/2020_2021.html